Jurnal Teknologi

Full Paper

# FERRIHYDRITE-CHITOSAN NANOCOMPOSITE AS A RECYCLABLE FLOCCULANT FOR PALM OIL MILL EFFLUENT

Juliana Jumadi[a], Azlan Kamari[a]*, Nurulsaidah Abdul Rahim[a], Norjan Yusof[b], I Wayan Sutapa[c], Sunardi[d]

[a]Department of Chemistry, Faculty of Science and Mathematics, Universiti Pendidikan Sultan Idris, 35900 Tanjong Malim, Perak, Malaysia
[b]Department of Biology, Faculty of Science and Mathematics, Universiti Pendidikan Sultan Idris, 35900 Tanjong Malim, Perak, Malaysia
[c]Department of Chemistry, Faculty of Mathematics and Natural Sciences, Universitas Pattimura, Ambon Maluku 97233, Indonesia
[d]Department of Chemistry, Faculty of Mathematics and Natural Sciences, Universitas Lambung Mangkurat, South Kalimantan 70714, Indonesia

**Article history**
Received
*7 April 2023*
Received in revised form
*12 November 2023*
Accepted
*28 November 2023*
Published Online
*18 February 2024*

*Corresponding author
azlan.kamari@fsmt.upsi.edu.my

## Graphical abstract

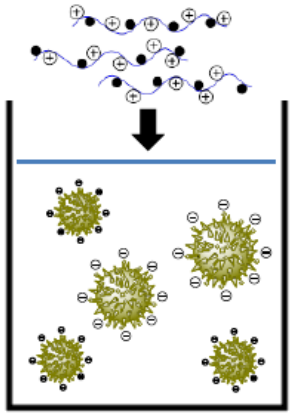

FCN added to POME

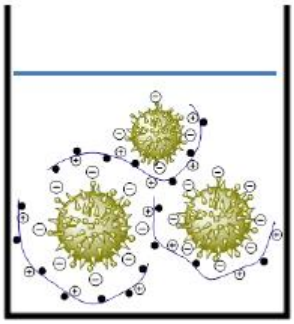

Charge neutralisation and polymer bridging mechanisms

## Abstract

In the present study, ferrihydrite-chitosan nanocomposite (FCN) was successfully produced by co-precipitation method and used for the first time as a recyclable flocculant for pre-treatment of palm oil mill effluent (POME). The physicochemical properties of FCN were studied using Raman spectrometer, Scanning Electron Microscope (SEM) and Thermogravimetric Analyser (TGA). The feasibility of FCN to remove total suspended solids (TSS), turbidity, chemical oxygen demand (COD), and, oil and grease (O&G) from POME was investigated using a jar test method. The optimum conditions for contaminant removal from POME were determined by varying the experimental parameters such as flocculant dosage, solution pH and settling time. The results obtained showed that FCN, at a dosage of 1.5 g/L, a contact time of 60 min and pH of 5.0 gave a highest reduction of turbidity, TSS, COD and O&G levels by 72.38%, 77.32%, 71.60% and 53.40%, respectively. Besides that, FCN exhibited a better flocculation performance as compared to alum and chitosan. After three cycles of flocculation/deflocculation process, FCN retained satisfying flocculation efficiency and flocculants recovery in the range of 80-83% and 43.2-78.6%, respectively. Combination of charge neutralisation and polymer bridging was the main key mechanism of interaction between FCN and POME contaminants. The synergy effect between iron oxide/oxyhydroxide nanoparticle and chitosan has increased the physicochemical properties and flocculation performance of the FCN nanocomposite. Overall, FCN nanocomposite can be used an alternative flocculant for POME treatment.

*Keywords*: Ferrihydrite-chitosan nanocomposite, flocculation, palm oil mill effluent, recyclable flocculant, wastewater treatment

## Abstrak

Dalam kajian ini, nanokomposit ferrihidrit-kitosan (FCN) telah berjaya dihasilkan melalui kaedah kepemendakan kimia dan digunakan buat kali pertama sebagai flokulan boleh dikitar semula untuk pra-rawatan efluen kilang kelapa sawit (POME). Sifat fizikokimia FCN dikaji menggunakan spektrometer Raman, mikroskop elektron pengimbas (SEM) dan penganalisis termogravimetri (TGA). Kebolehlaksanaan FCN untuk menyingkirkan jumlah pepejal terampai (TSS), kekeruhan, permintaan oksigen kimia (COD), dan, minyak dan gris (O&G) daripada POME telah diselidik

menggunakan kaedah ujian balang. Keadaan optimum untuk penyingkiran bahan cemar daripada POME ditentukan dengan mempelbagaikan parameter eksperimen seperti dos flokulan, pH larutan dan masa mendap. Keputusan yang diperolehi menunjukkan bahawa FCN, pada dos 1.5 g/L, masa sentuhan 60 min dan pH 5.0 memberikan pengurangan tahap kekeruhan, TSS, COD dan O&G tertinggi sebanyak 72.38%, 77.32%, 71.60% dan 53.40%, masing-masing. Selain itu, FCN mempamerkan prestasi flokulasi yang lebih baik berbanding tawas dan kitosan. Selepas tiga kitaran proses flokulasi/deflokulasi, FCN mengekalkan kecekapan flokulasi yang memuaskan dan pemulihan flokulan dalam julat 80-83% dan 43.2-78.6%, masing-masing. Gabungan peneutralan cas dan penyambungan polimer adalah mekanisme utama interaksi antara bahan cemar FCN dan POME. Kesan sinergi antara nanopartikel ferum oksida/oksihidroksida dan kitosan telah meningkatkan sifat fizikokimia dan prestasi flokulasi nanokomposit FCN. Secara keseluruhannya, nanokomposit FCN boleh digunakan sebagai flokulan alternatif untuk rawatan POME.

*Kata kunci*: Nanokomposit ferrihidrit-kitosan, flokulasi, efluen kilang kelapa sawit, flokulan boleh dikitar semula, rawatan air kumbahan



## 1.0 INTRODUCTION

POME is a liquid waste product of the palm oil extraction process [1]. It was predicted that over 50.55 million tonnes of POME would generated annually from the processing of crude palm oil in global, because each tonne of crude palm oil generally yields around 0.5-0.73 tonnes of POME [2, 3]. Total suspended solids (TSS), oil and grease (O&G), biochemical oxygen demand (BOD), and chemical oxygen demand (COD) values are all high in untreated POME. It also has a high concentration of nutrient and organic matter, which normally do not comply the regulation criteria for direct discharge [4, 5]. If the discharge and disposal of POME or by-products into water streams are not adequately handled, they can cause major water pollution, pose a health risk to humans, and constitute a nuisance owing to an unpleasant odour. POME will turn the colour of water streams brown, make them stink, slimy and may kill aquatic species life. Indeed, the source of drinking water will be contaminated as a result of the increase in BOD in POME, as well as a decrease in dissolved oxygen (DO). This scenario can be described by bacteria's high oxygen consumption, which leads in a significant decrease in the amount of DO present in the aquatic environment [6, 7]. Given the importance of water resources, it is critical to ensure that the appropriate procedures are implemented to protect the water resources against POME pollution.

Ponding system is the most commonly used method for treating POME. However, this conventional approach did not meet the regulatory standard's requirements, which required a vast treatment area, long retention time treatment and the production of an objectionable odour [8, 9, 10]. As a result, flocculation treatment has emerged as a viable alternative to overcome the limitations of the conventional method of POME treatment. The flocculation method is frequently employed in wastewater treatment because of its capability to destabilise and aggregate colloids [11]. There are many reasons why flocculation is one of the most popular solid–liquid separation strategies compared to other conventional treatment methods. It is a cost-effective technology that is easy to operate and produces far less solid waste than any alternative method that has been utilised in the past. According to a Scopus citation report, the total number of publication using keyword flocculation has increased from 23,239 in 2014 to 37,741 in 2024.

Nowadays, studies related to chitosan-based materials have become one of the main focuses of developing environmentally friendly materials especially in water and wastewater treatment [12, 13]. Chitosan and chitin are known to have outstanding properties, such as biocompatibility, biodegradability, non-toxic, and non-allergenic, while possessing some unique properties like film forming ability, chelation and absorption properties, as well as antimicrobial characteristics. In the near decades, various applications of chitosan for the environment have been reported practically in food preservation [14], pesticide [15], fertiliser [16], soil remediation [17] and air pollution [18]. Chitosan contains a large number of amino and hydroxyl groups, which are important for chelating effects. This makes chitosan a promising coagulant or flocculants in water and wastewater treatment [19, 20].

Over the past two decades, the outstanding performance and advantages of using iron oxide/oxyhydroxide nanomaterials have gained the attention of research society in solving the environment related problems. As for iron-based nanomaterials (e.g. ferrihydrite, goethite, hematite and magnetite), they have recently also shown outstanding adsorption capacity for removing heavy metals, dyes [21], inorganic and organic compounds [22]. This is due to their excellent properties such as large specific surface area, high porosity, strong magnetic response, biocompatible and reusable, which results in an extraordinary sorption capacity [23]. Moreover, they can coordinate with other elements due to their variable oxidation states.

The capability of pure chitosan and iron-based materials for coagulation and flocculation in water or wastewater treatment is undeniable. However, they

have several drawbacks in terms of removing the flocs after the treatment process and iron oxide/oxyhydroxide tends to aggregate due to their large surface-to-volume ratio and low surface energy [24]. Moreover, the pure iron oxide/oxyhydroxide nanoparticles have high chemical activity, which easily oxidised in the air (especially magnetite) that generally results in the loss of magnetism and dispersibility. Therefore, providing a proper surface coating and developing some effective protection strategies to maintain the stability of magnetic iron oxide/oxyhydroxide nanoparticles is very important. Practically, it is worthwhile that in many cases, the protecting shells (biopolymer) not only stabilise the iron oxide/oxyhydroxide nanoparticles, but can also be used for further functionalisation [25].

The iron oxide/chitosan nanocomposites were being explored for various applications, including drug delivery [26], tissues engineering [27] and water/wastewater treatment [28]. Iron oxides come in a variety of forms, such as ferrihydrite, magnetite, hematite, goethite and etc. Iron oxides such as magnetite and hematite are commonly utilised in composites with other materials. According to the previous studies on water/wastewater treatment, the iron oxide/chitosan nanocomposites had shown a great performance in terms of adsorption capabilities, biocompatibility, magnetic properties, antibacterial, and regeneration [29, 30]. Previous researches have frequently shown the application of hematite/chitosan and magnetite/chitosan nanocomposite in water and wastewater treatment. Thus, it is imperative to assess the potential of other form of iron oxide which is ferrihydrite/chitosan nanocomposite to reduce contaminants in wastewater.

Therefore, the ultimate objective of the present work was to evaluate the potential and effectiveness of FCN as a flocculant to reduce the turbidity, TSS, COD and O&G, in comparison with alum and chitosan. A series of batch flocculation studies were carried out in order to determine the optimal flocculant dosage, solution pH of the system and settling time. Finally, this study also aimed to study the regeneration and recyclable potential of the FCN. Thus, POME pre-treatment could be improved in a more cost-effective and environmentally friendly manner.

## 2.0 MATERIALS AND METHODS

### 2.1 Materials

Chitosan powder (99% deacetylated, MW 33 kDa) and iron(III) chloride hexahydrate ($FeCl_3.6H_2O$) were purchased from Acros Organic and Bendosen Laboratory Chemicals, respectively. Aluminum sulfate (alum, $Al_2(SO4)_3$) was supplied by Sigma-Aldrich. Sodium dodecyl hexahydrate (SDS, $NaC_{12}H_{25}SO_4$) was purchased from Fisher Chemical. For pH adjustment, hydrochloric acid (HCl) and sodium hydroxide (NaOH) were acquired from Merck and diluted to 1 M using deionised water. All chemicals were of analytical grade and used as received without further purification.

The POME was obtained from a palm oil mill located at Trolak, Perak, Malaysia. Since the fresh POME has a temperature ranging between 75-90 °C, it was allowed to cool to around 40-45 °C before being collected into polyethylene bottles. The sample was kept at a low temperature (4 °C) in an airtight bottle to prevent biodegradation due to microbial activity. Table 1 lists the method that was performed to characterise the POME sample for this study.

**Table 1** Physicochemical parameters of raw POME and method analysis for water quality testing

| Parameter (unit) | Concentration Value* | Method/ Instrument |
|---|---|---|
| pH | 4.67 ± 0.05 | Thermo Scientific Orion 2-Star pH Meter |
| Turbidity (NTU) | 37,450 ± 1,040 | Hach 2100P Turbidimeter |
| TSS (mg/L) | 19,694 ± 714 | 2540 D. TSS Dried at 103-105 °C |
| Oil and grease(mg/L) | 6.166 ± 261 | Hexane Extractable Gravimetric Method |
| COD (mg/L) | 60,100 ± 3,460 | 5220 COD Method |

*Average ± standard deviation of three replicates.

The physicochemical parameters of POME were measured by using the recommended method suggested by APHA (American Public Health Association) Standard Method Examination of Water and Wastewater. All analyses were carried out in triplicates.

### 2.2 Preparation of Ferrihydrite Nanoparticles

Briefly, 100 mL of a 0.2 M $FeCl_3 \cdot 6H_2O$ solution was prepared and placed in a 250 mL beaker. The solution was vigorously agitated while a 1 M NaOH solution was added drop by drop until the pH hit 12. The suspension was centrifuged and then rinsed with deionised water several times before being freeze dried. Theoretically, when the $FeCl_3$ and NaOH solutions are mixed together, the substitution of -OH groups on the resin substrate with chlorides ions (Cl) from solution results in the formation of $Fe(OH)_3$, with no additional secondary phase forming under supersaturation conditions. However, because $Fe(OH)_3$ is unstable in water, the precipitated phase is expected to form after the ion exchange process and also the expected formation of ferrihydrite [31]. The reaction described above can be substituted by the following:

$$FeCl_3 + 3NaOH \rightarrow \text{ferrihydrite} + 3NaCl$$

### 2.3 Preparation of FCN

Basically, 2.0 g of SDS was dissolved in 400 mL of ionised water, and then 0.25 g of ferrihydrite nanoparticles was added into the SDS solution with intensive stirring at room temperature (26 ± 2 °C). Subsequently, 0.25 g of chitosan powder was dissolved in 100 mL of 1% (w/v) acetic acid solution, and then slowly dropped the chitosan solution into the ferrihydrite nanoparticle and SDS surfactant solution. At room temperature, the mixture was continuously stirred at a constant speed for one hour. Then, the expected FCN was separated from the solution and thoroughly washed several times with deionised water and ethanol. The precipitate was collected and dried at 50 °C until a constant weight was obtained [32].

### 2.4 Characterisation of FCN

Raman spectra were obtained using a Renishaw inVia Raman Microscope equipped with a 1800 g/mm of holographic grating and an Olympus metallurgical microscope to focus the laser beam and collect the scattered light from the sample. The Raman scattering experiment was carried out with a He-Ne laser at wavelength of 633 nm and the time of exposure was 30 s with a range of spectrum within 100 to 1500 $cm^{-1}$.

The morphology and surface structures of the precursor and nanocomposite were examined by using a Hitachi SU 8020 VHR Field Emission Scanning Electron Microscope that is equipped with an energy dispersive X-ray spectrometer (EDX) to get elemental composition information. The samples were first coated with platinum to avoid electron charging by using Automatic Platinum Sputter Coater System (Quorum Q150RS).

The thermal stability of the materials was studied using a Mettler Toledo Thermogravimetric Analyzer, model TGA/DSC 1 instrumentation. The thermal deterioration was carried out under an argon environment at a heating rate of 10 °C per min from 25 to 900 °C. The purging gas was fixed at a flow rate of 20 mL/min.

The point of zero charge ($pH_{PZC}$) was used to determine the net charge on the material surface. The $pH_{PZC}$ analysis was carried out by using the salt addition method. In a series of 250 mL conical flasks, 0.1 g of FCN was added to 50 mL of 0.1 M $NaNO_3$ solution to maintain the ionic strength of the solution. A solution of diluted HCl and NaOH was added to adjust the solution's initial pH ($pH_i$) in the range between 2 and 11. The samples were shaken for 24 h at room temperature using a Protech Orbital Shaker Model 720 at 150 rpm. After settling, the final pH ($pH_f$) of the supernatant was recorded. Graph of ΔpH (ΔpH = $pH_f$ – $pH_i$) against $pH_i$ to determine the $pH_{pzc}$. Each set of experiments was performed in triplicate and the mean value was recorded.

### 2.5 Flocculation Studies

In this study, prior to beginning the flocculation performance, the POME samples were homogeneously mixed and then separated into beakers containing 500 mL of each sample solution. After the flocculants had been added to each beaker, they were swirled for 3 mins at a constant speed of 250 rpm using jar tester to ensure that the flocculants were evenly distributed throughout the POME sample. Once this is accomplished, drop the stirring speed to 50 rpm, and continue mixing for a further 30 mins. The purpose of this slower mixing speed was to increase flocs production by increasing particle collision, which results in larger flocs being formed.

In the following 75 mins, the system is allowed to settle into a quiescent state under the influence of an external magnetic field. Finally, the value of turbidity, TSS, COD, and O&G content measurement, which represents a final concentration, may be achieved by collecting the sample at a depth of 2 cm beneath the surface of the water. The experiment was carried out at a room temperature ranging between 25-30 °C.

### 2.6 Regeneration and Recycling Test

For the purpose of reducing treatment costs, regeneration and recycling test was carried out to separate the FCN from the POME contaminant/pollutant. The resultant FCN flocs were first centrifuged at 4000 rpm for 10 minutes to separate the composite from the trap contaminant. Following that, it was immersed in 1.0 mL NaOH with a pH of 9 for 10 minutes before being subjected to ultrasonic treatment for another 10 minutes. Until this point, it was expected that the composites would separate from the POME contaminant/pollutant.

Approximately 2 mL of acetone was added to the regenerated nanocomposite mixture, which was then ultrasonically processed for 10 mins before being rinsed multiple times with methanol. Finally, the regenerated FCN flocculants were collected, dried and ready to be reused. Based on preliminary study, there was no obvious change (± 2%) in percentage of removal contaminant after three cycles of flocculation and deflocculation. Therefore, the flocculation and deflocculation was set for three cycles. The removal efficiency of TSS, O&G, and turbidity determined for each cycle.

## 3.0 RESULTS AND DISCUSSION

### 3.1 Flocculation Study

A number of tests such as flocculant dosage, solution pH and settling time were carried out in order to determine the optimal factors that lead to the best flocculation efficiency. The performance of FCN, chitosan and alum as flocculants in treating POME was investigated using jar testing method. Contaminant removal including turbidity, TSS, COD and O&G will be measured as an indicator of the flocculation capacity.

### 3.1.1 Effect of Flocculant Dosage

During the course of the study, it was discovered that dosage was one of the most significant elements to consider in order establishing the optimum conditions for performing the flocculant in the flocculation process. More specifically, inadequate or excessive dosing would result in poor performance during the treatment procedure, as previously stated [33]. Furthermore, it was necessary to find the optimal dosage in order to lower the dosing cost while still attaining the best potential treatment results in terms of efficacy and efficiency.

For the purpose of evaluating the influence of flocculant dosage on the percentage removal of contaminants, we varied the dose of flocculant from 0.50 to 2.5 g/L. The pH of the POME sample was tested at its original pH and after 75 minutes of settling time, the effect of dosage was explored, and the findings are given in Figure 1.

Based on the results, the percentage removal of contaminant rose as the flocculant dosage was raised until it reached a maximum value for the FCN. At the maximum point, the performance drop is marginally exacerbated with each additional dosage of flocculants. When the dose of FCN polymer flocculants is gradually increased, the strength of the repulsive force between the particles weakens as the charge neutralisation point is reached. This suggests that flocculation mechanism is based on charge neutralization [34]. It was also revealed that the trends in TSS and turbidity were almost the same, but with a different percentage of removal for contaminant were investigated. To put it another way, the turbidity level will rise in direct proportion to the increase in TSS in the sample.

From Figure 1, the FCN showed the greatest percentage reduction in parameters for applied dosage at 1.5 g/L, corresponding to 71.83% in turbidity, 80.49% in TSS, 72.57 % in COD, and 47.56 % reduction in O&G removal. At the same dosage, alum results in the lowest decrease in turbidity, TSS, COD and O&G, with 36.01%, 37.55%, 40.28% and 29.73%, respectively. In general, ferrihydrite combined with chitosan polymer produced a great synergistic effect that resulted in a larger percentage of pollutants being removed from the solution. It was discovered that the optimum dosage of FCN, chitosan and alum in this study was 1.5 g/L, 2.0 g/L and 2.5 g/L, respectively.

The flocculation performance using the synthesised FCN could be explained based on charge density. As the charge density of the polymer grew, the adsorption of coagulants and flocculants increased as well [35]. For ferrihydrite, the incompletely metal cations on the iron oxide surface acting as electron accepting Lewis acid sites, it will be possible to selectively remove Lewis basic compounds from the surface by building a coordination bond with the ferrihydrite surface, lead to the better flocculation performance [36]. While for chitosan, at acidic circumstances, the amines get protonated and become positively charged, resulting it to becoming a water-soluble cationic polyelectrolyte. However, when exposed to a basic environment, the amines in chitosan become deprotonated, resulting in the polymer losing its charge and becoming insoluble.

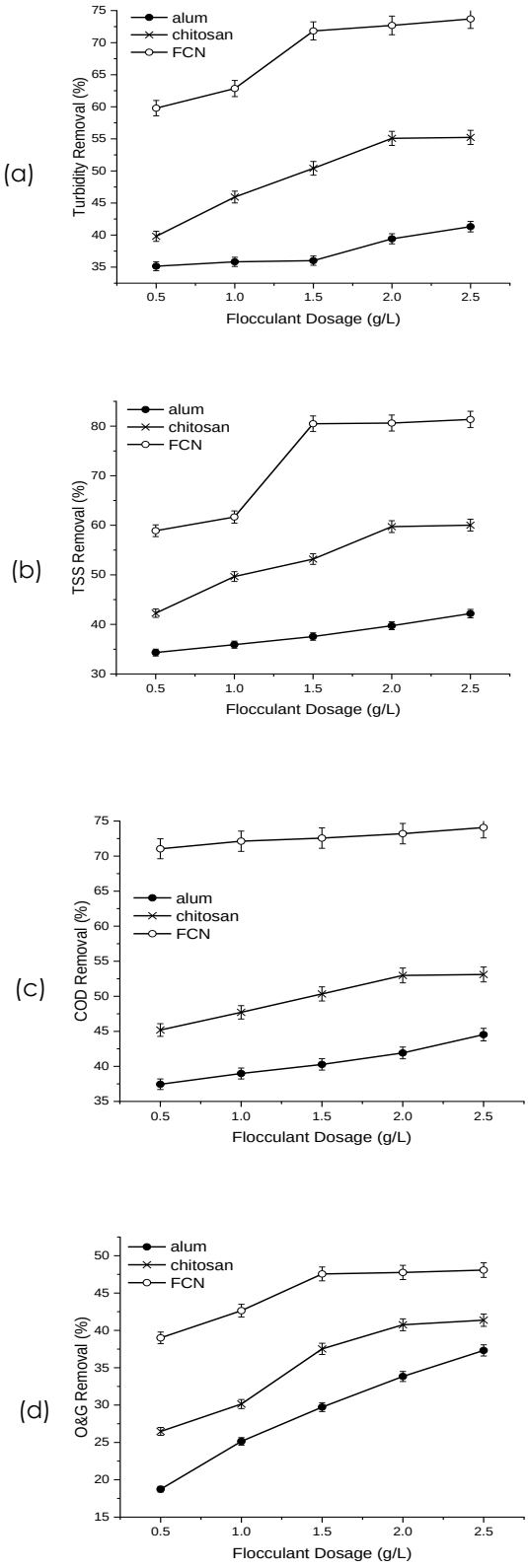


**Figure 1** Effect of dosage on percentage removal of(a) turbidity, (b) TSS, (c) COD and (d) O&G (pH = original POME sample, Settling time = 75 min)

The presence of amino groups further demonstrates that the pH of chitosan has a significant impact on the charged state and characteristics of the polymer [35,36].

Basically, POME is a naturally acidic suspended effluent, and FCN could be used to destabilise the pollutant present in POME. The FCN appears to have an additive effect; almost multiple contaminants are being eliminated at the same time by the materials. The amine functional groups in chitosan, as well as the positively charged iron oxide, aid in the destabilisation and adsorption of the contaminant, which is negatively charged in POME. Furthermore, the increase in percentage removal was also associated with an increase in the total area and active site of $Fe^{2+}$ and $Fe^{3+}$ for organic compound adsorption [37]. This indicates that the particles are rapidly destabilised based on charge density of the flocculant, and it can also be stated that the amount of flocculant necessary to destabilise the particles is less for a flocculant with a greater charge density.

Both the amino groups of chitosan and the ferrihydrite particle are protonated when they are placed in an acidic solution. Upon immersion in acidic solution, the FCN develops a strongly positive charge, which allows the iron oxide-chitosan to form ionic or hydrogen bonds with surfaces that are negatively charged. This will further reduce or neutralise the particle surface charge. As a result, the destabilisation of particles caused by FCN may be explained by a charge neutralisation mechanism.

In contrast, as with alum, the contaminant and colloids removal performance of the coagulant exhibits a modest increase with increasing dosage, indicating that the flocculation performance has deteriorated. Charge reversal and possible destabilisation of colloid particle may have occurred when raising the alum dosage, as a result of the possibility of a considerable fall in pH of the POME at high flocculant dosage was used (33). The coagulation–flocculation process for aluminum-based coagulants has mostly evolved around a charge neutralisation mechanism. Especially for coagulants containing a significant proportion of monomeric aluminium species, the contaminant must be of sufficient size to form nuclei on the surface of the coagulant.

### 3.1.2 Effect of Solution pH

An investigation into the influence of solution pH was carried out utilising fixed experimental conditions: a flocculants dosage of FCN (1.5 g/L), chitosan (2.0 g/L), alum (2.5 g/L) and a 75 minute settling time for a pH range ranging from 4 to 9. In general, the results revealed that the recommended solution pH for FC nanocomposite, chitosan and alum was observed to be pH 5, 6 and 7, respectively. At the initial pH of 5, FCN is possible to obtain about 71.25%, 77.49%, 68.49%, and 48.65% reductions in turbidity, TSS, COD, and O&G, respectively. However, the removal of COD and O&G are not influence by the effect of pH generally.

For removal of O&G from the POME, FCN demonstrated a high capability for O&G removal at the initial pH value. As illustrated in Figure 2, when the pH was raised to a greater level, the O&G removal was significantly reduced as compared to the acidic condition. It is considered that this circumstance provides a greater opportunity for particle restabilisation due to reversal of surface charge when compared to when the pH is raised to a higher level. It is well known that exposure to severe acidic conditions resulted in the formation of extremely strong cationic charges on chitosan as well as on ferrihydrite nanoparticles. As a result, we can conclude that the acidic conditions of POME promote the elimination of O&G.

The pH of POME was originally between 4.5 and 4.8; it was determined that the O&G removal was extremely satisfactory around the pH of POME's original composition. This encouraging fact could bring to a conclusion that pH adjustment on POME in the real treatment system can be discarded in order to remove the residue oil by using any of these coagulants and/or flocculants. At the high acidic state exacerbates POME's ability to shatter oil droplets and destabilise suspended solids in the solution [38,39]. Therefore, the electrostatic attractions between residue oil molecules and adsorption site increase and indirectly increase the adsorption of residue oil onto chitosan.

Besides that, one of the most important intrinsic characteristics of FCN polymer flocculants that influences their flocculation effectiveness is their surface charge property. The issue can also be interpreted in terms of the material's point of zero charge. According to Maćczak *et al*. [34], the point of zero charge implies that van der Waals attraction between cation flocculants and anion colloids particles is operating at its highest pace. When the pH of the solution was lower than the $pH_{PZC}$, the cation present in flocculants was protonated as a result of the strong electrostatic force present in suspension. Furthermore, at a certain extent, electrostatic force becomes insufficient to resist the strong van der Waals attraction, resulting in the deprotonation of the positive charge of flocculants.

Figure 3 depicts the curve of the point of zero charge ($pH_{PZC}$) of the FCN in solution. The graph clearly demonstrates that the charge on the FCN surface is correlated to the pH of the solution with $pH_{PZC}$ of FCN less than 6. In other words, when the pH of the solution is lower than $pH_{PZC}$, the FCN is positively charged, and vice versa when the pH of the solution is greater than $pH_{PZC}$. For POME, it literally has a negatively charge which is mostly due to colloidal particles derived from hemicellulose and extractives components in the composition of the POME [40]. This discovery was consistent with the findings of Ganapathy *et al*. [41], who investigated the POME in the same way. When the zeta potential is decreased to zero, the best flocculation will be accomplished since there will be no electrostatic repulsion between the particles in solution.

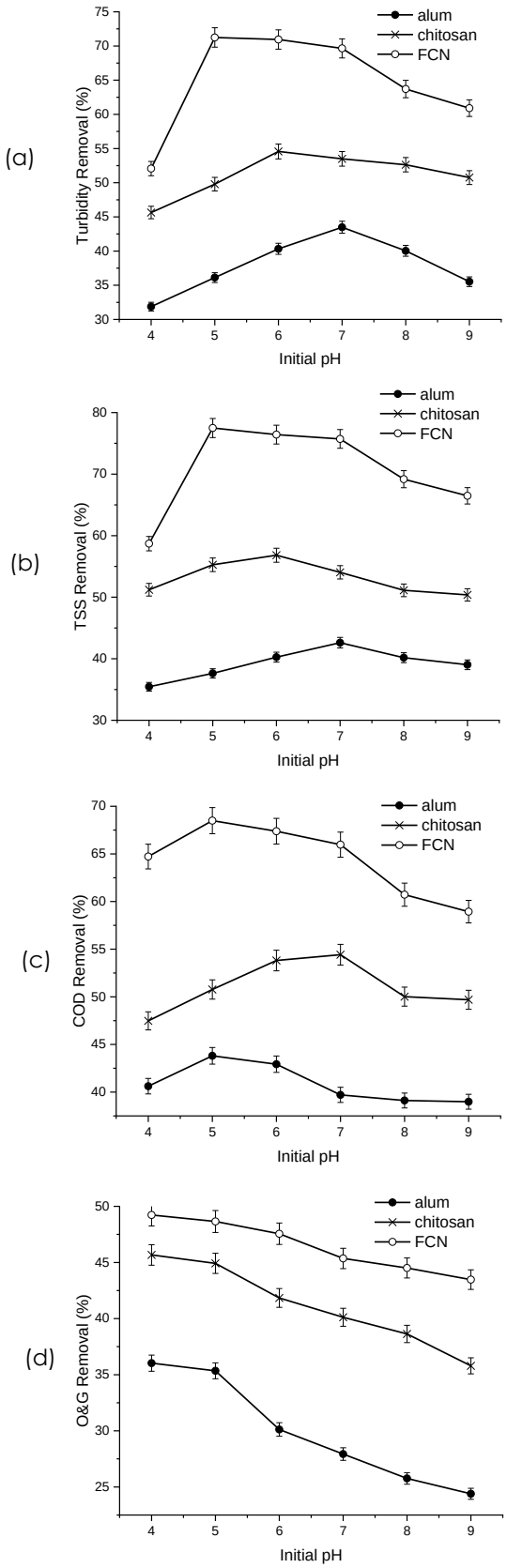


**Figure 2** Effect of solution pH on the percentage removal of (a) turbidity, (b) TSS, (c) COD and (d) O&G (Dosage = 1.5 g/L of FCN, 2.0 g/L of chitosan, 2.5 g/L of alum, Settling Time = 75 min)

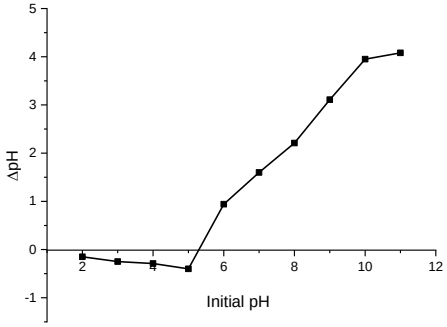


**Figure 3** $pH_{PZC}$ plot for FCN

### 3.1.3 *Effect of Settling Time*

Typically, adequate time must be allowed for the production of particles with a size that is large enough to permit for their efficient removal during the sedimentation process, In the present study, settling time was varied from 15 to 75 min. Figure 4 depicts the changes in turbidity, TSS, COD and O&G with regard to settling time. From the application of the FCN in this present study, the highest percentage reduction of parameters at settling time 60 min corresponding to 72.38%, 77.39%, 71.59% and 53.37% for turbidity, TSS, COD and O&G, respectively.

From the results, it was discovered that the removal of all contaminants followed a similar pattern with the percentage removal increasing as the settling period was prolonged until it reached an optimal duration and showed no discernible difference. According to the results, this was most likely due to the fact that all contaminants were strongly absorbed into the flocs created with the assistance of chitosan and iron oxide-based components. In addition, the combination of the two materials chitosan and iron oxide nanoparticles would result in extremely high attraction forces between contaminating particles, resulting in strong flocculation performance that could have a positive impact on the final product.

According to the present finding, the FCN sediments show a significantly faster rate. 60 minutes of sedimentation can remove approximately 70% of the pollutants present in POME. Using FCN, colloids aggregate more quickly, allowing for the construction of bridges and charge neutralisation between pollutants, as well as the generation of particles of sufficient size that can settle more quickly and easily. The value of TSS decreases when the bridging particles and flocs begin to descend to the bottom of the beaker, and this impact is mostly influenced by the gravitational force acting on the particles. According to Yu *et al*. [42], magnetic flocculation can be used to increase the size and pace of growth of flocs by the combination of charge neutralisation and bridging flocculation mechanism. In the flocculation separation process, the results reveal that the magnetic flocculation separation has a significant anti-interference capacity.

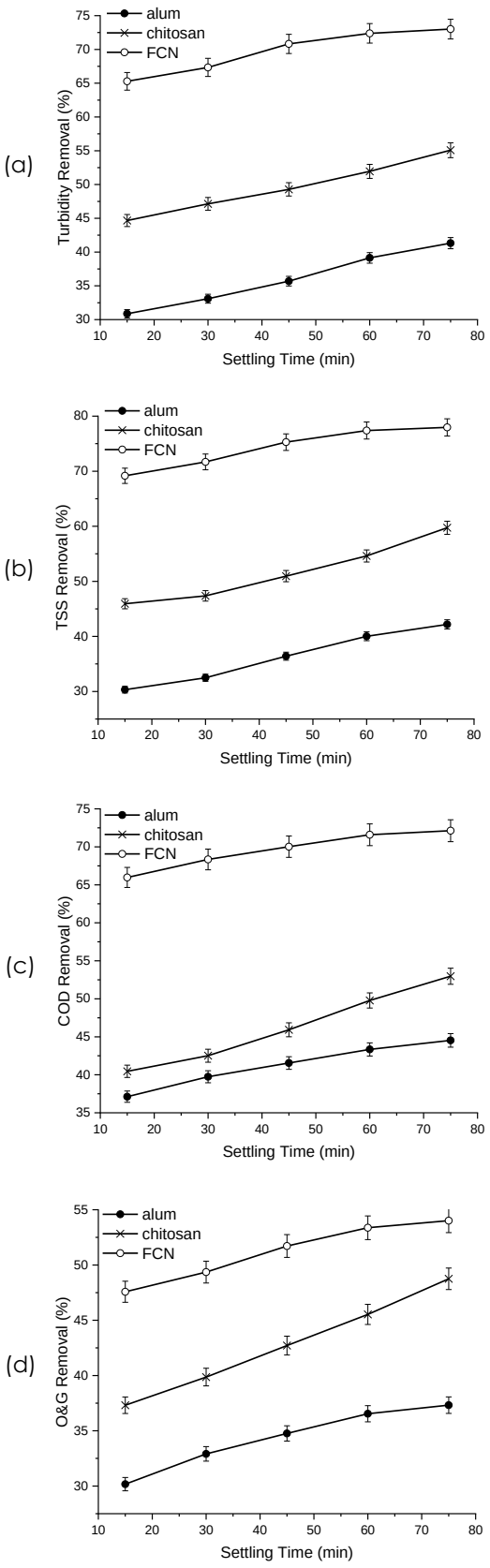


**Figure 4** Effect of settling time on the percentage removal of (a) turbidity, (b) TSS, (c) COD and (d) O&G (Dosage = 1.5 g/L of FCN, 2.0 g/L of chitosan, 2.5 g/L of alum, pH =5)

## 3.2 Characterisation Study

### *3.2.1 Raman Analysis*

Figure 5 depicts the Raman spectra of ferrihydrite, chitosan and FCN. Synthesised ferrihydrite powder exhibits three prominent broad and weak bands at 349, 524 and 1362 $cm^{-1}$, with the strongest intensity bands at 794 $cm^{-1}$. As shown in Table 2, the Raman analysis of synthesis ferrihydrite was found to be very close to and in good agreement with the characteristic band reported by the previous researchers, which can be used to confirm the purity of the ferrihydrite before it is further coupling with chitosan.

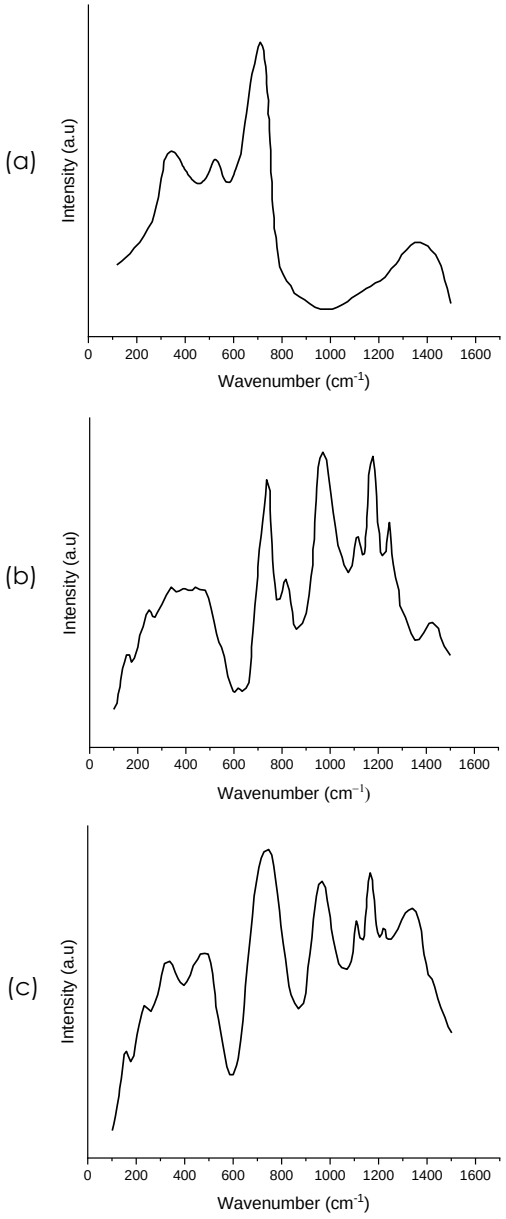


**Figure 5** Raman spectra of (a) ferrihydrite, (b) chitosan and (c) FCN

The Raman spectrum of chitosan displays characteristic bands at 965 $cm^{-1}$ (CN), 1050-1200 $cm^{-1}$ (CC), 1290-1350 $cm^{-1}$ (CNH) and 1430 $cm^{-1}$ (amide-III) [43,44]. In comparing the Raman spectra of the FCN, obviously a slight difference was observed. The spectrum of nanocomposite is the combination of ferrihydrite and chitosan peaks band. Again, this suggests that physically bond linkages are being formed between the two materials precursor.

**Table 2** Raman shift wavenumber ($cm^{-1}$) of ferrihydrite nanoparticle reported by previous researchers

| Iron oxide | Wavenumber ($cm^{-1}$) | Reference |
|---|---|---|
| Ferrihydrite | 361(w), 508(w), 707(s) | Das *et al*. [45] |
| | 223(s), 288(s), 390(s), 607(w) | Rout *et al*. [46] |
| | 370(w), 510(w), 710(s) | Hanesch [47] |
| | 370(w), 510(w), 710(s), 1340(w) | Mazetti and Thistlethwaite [48] |

### 3.2.2 SEM Analysis

Figure 6a presents image micrograph of synthesised ferrihydrite that show irregularities in spherical shape with 10 to 20 nm of particle sizes. As can be seen in the SEM image, the ferrihydrite nanoparticle shows a slightly aggregation or agglomeration due to the strong supersaturation of very small nanoparticle [49]. There are several factors that influence the particle size of synthesised ferrihydrite, including the rate of alkali addition, the concentration of iron precursor, and the aggregation effect.

The surface structure of chitosan is flat and smooth, with no sign of porosity on the surface [50, 51]. While for FCN, the surface morphology of both the precursor ferrihydrite and the chitosan was clearly altered. The surface of the nanocomposite is a blend of flat and spherical surfaces, which represent the presence of the ferrihydrite and chitosan materials, respectively, on the surface of the nanocomposite, as well as the creation of discrete aggregates on their surfaces after being composite with ferrihydrite nanoparticle (Figure 6b).

The results of the SEM analysis of FCN demonstrate that the spherical shaped of ferrihydrite nanoparticle are distributed equally across the chitosan surface, which is consistent with the observation made by Rabel *et al*. [52]. Aside from that, chitosan particle condensation was found in some locations, which may have occurred as a result of a ferrihydrite interaction between chitosan particle clusters. Another factor that contributed to the success of the ferrihydrite and chitosan combination was the reduction in the size of FCN when compared to precursor ferrihydrite nanoparticles.

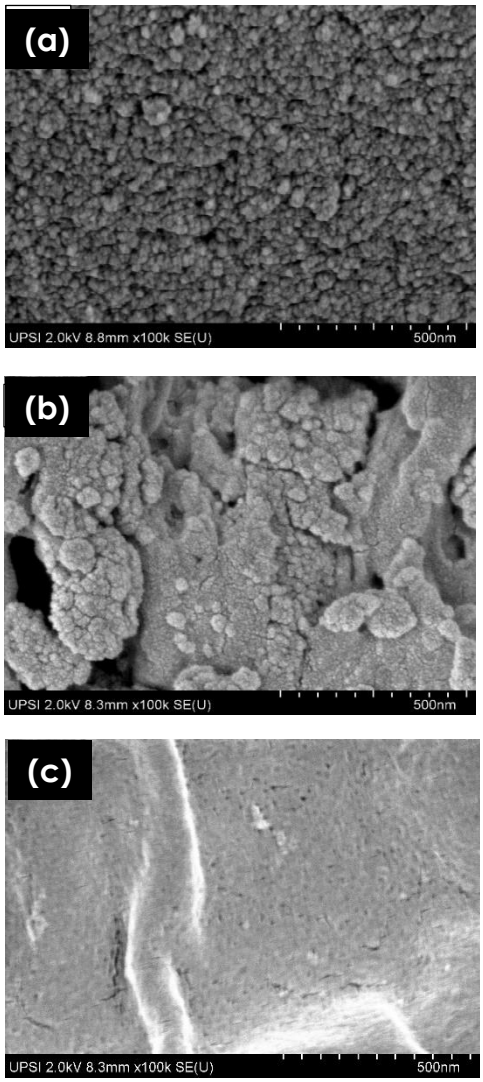


**Figure 6** SEM images of (a) ferrihydrite, (b) FCN before flocculation and (c) FCN after flocculation

After flocculation, the image after the POME uptake has transformed the surface of the FCN become wavy, some are clumped together, and there is also a glossy white strip attributable to the uptake of fat and oil in the composite (Figure 6c). Asadpour *et al*. [53] reported a similar observation, in which the shining white strip was assigned to the oil adsorption on the surface of mangrove bark. Generally, we have learned that the raw POME combination is composed of 95-97% of water, 0.6-0.7% of oil, and 4-5% of total solids, primarily consisting of debris from the fruit [54]. When the exterior of the particle is smooth and uneven, it indicates that the particles are being held together by the natural viscosity and thickness of the adhering oil.

### 3.2.3 TGA Analysis

Figure 7 depicts the TGA curves for ferrihydrite, chitosan and FCN before and after flocculation. For ferrihydrite (Figure 7a), the peak observed below 300 °C, corresponding to an 18.79 % weight loss of, indicated that the surface $H_2O$ groups on ferrihydrite had been removed without causing structural damage to the material. The conclusion of the dehydration/dehydroxylation process, which results in the crystallisation of hematite, was signalled by the occurrence of an event at 484 °C of peak temperature. The modest loss observed at temperatures ranging from 300 to 1000 °C suggests that ferrihydrite has undergone a complete phase change into hematite.

The TGA of chitosan reveals two stages of deterioration (Figure 7c). The first stage occurred at temperatures ranging from 40 to 150 °C and resulted in a 10 % weight loss, which corresponds to the loss of water or moisture adsorption on the chitosan surface. The splitting of polysaccharide rings occurs in the second stage of degradation, at temperature range of 220-550 °C, resulting in a weight loss of 65.44 %.

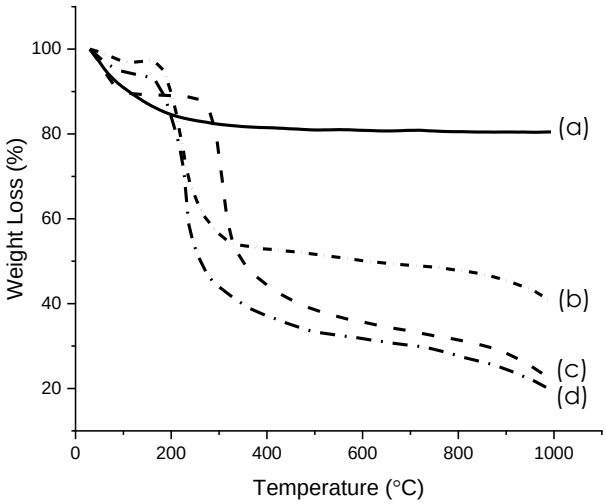


**Figure 7** TGA analysis of (a) ferrihydrite, (b) FCN before flocculation, (c) chitosan and (d) FCN after flocculation

In general, FCN exhibits three stages of degradation that can be examined (Figure 7b). The initial phase of weight reduction is the discharge of fluids from the body surface. The decomposition of the chitosan polymer is attributed to the second stage of the process. And the final step is characterised primarily by composite carbonisation as well as the disintegration of residual materials [55]. The degradation yield also appears to increase at a rate that is more than the weight percentage of chitosan in the nanocomposite, showing that the ferrihydrite has an effect on the nanocomposite stability [56,57].

Following the flocculation of FCN with POME (Figure 7d), the weight loss of the first stage is generally caused by the evaporation of the free moisture and the binding of the bound moisture, which results in POME sludge. Next, the decomposition of complex organic structure constitutes the second step of weight loss. Carbon-containing molecules in POME sludge have been degraded because the C-C bond has been broken, resulting in the production of $H_2$, $CH_4$, $CO_2$, and CO [58]. This phenomenon occurs as a result of the aliphatic chemicals, carbohydrates, and protein degradation from the POME sludge attaching to the surface of composites.

At this stage, because the majority of the components are volatile, the material shows a significant weight loss in conjunction with the production of gas [59]. Finally, the phase of breaking of iron oxide and chitosan bonding is represented by the third weight loss phase of the TGA curve. The decomposition and deterioration of the hydrogen bond between the amino group of chitosan and the hydroxyl group of iron oxide is described here. It is possible that the degradation of the chitosan in the composite is responsible for the bond breakage at this stage. As previously stated, the chitosan exhibits greater thermal breakdown as compared to the iron oxide in the prior TGA analysis.

## 3.3 Regeneration and Recycling Test

When it comes to maintaining resource reutilisation, the regeneration and reuse of flocculants are considered to be an alternative strategy that adheres to the concepts of sustainable production. Due to the fact that the results of the previous experiment indicated that flocculation was caused by charge neutralisation and bridge interaction, pH shift was identified as a deflocculation mechanism to release flocculants from the contaminant flocs. From Table 3, the surface of the flocculants will become increasingly uncharged under a high pH condition, which will in turn cause the spent of iron oxide-chitosan flocculants to desorb the contaminant molecules.

A conformational changed for the soluble behaviour of the flocculants when hydrophobic groups cause aggregation of the polymer chains. Therefore, by selecting the appropriate pH conditions, it is possible to achieve both binding and releasing anionic contaminant. As a result, in order to assess the recyclability of regenerated flocculants for use in a subsequent POME treatment process, the regeneration of flocculants from flocs was carried out by filtration at a pH of 9, and the results are shown in Table 3.

The aforementioned scenario will lead to a conformational change for the soluble behaviour of the flocculants when hydrophobic groups cause aggregation of the polymer chains. Therefore, by selecting the appropriate pH conditions, it is possible to achieve both binding and releasing anionic contaminant. As a result, in order to assess the recyclability of regenerated flocculants for use in a subsequent POME treatment process, the regeneration of flocculants from flocs was carried out by filtration at pH 9, and the results are shown in Table 3.

**Table 3** Effect of regeneration cycles on contaminant removal in POME

| Contaminant | *Regen. cycles | Recovery of | Contaminant |
|---|---|---|---|
| Turbidity | 0 | - | 71.0 ± 2.8 |
| | 1 | 83 ± 6 | 70.7 ± 2.2 |
| | 2 | 80 ± 5 | 69.9 ± 3.5 |
| | 3 | 82 ± 5 | 67.2 ± 4.1 |
| TSS | 0 | - | 78.6 ± 3.1 |
| | 1 | 83 ± 6 | 78.1 ± 2.7 |
| | 2 | 80 ± 5 | 77.7 ± 2.5 |
| | 3 | 82 ± 5 | 74.2 ± 3.2 |
| O&G | 0 | - | 46.2 ± 4.8 |
| | 1 | 83 ± 6 | 45.9 ± 5.4 |
| | 2 | 80 ± 5 | 45.0 ± 5.1 |
| | 3 | 82 ± 5 | 43.2 ± 4.2 |

*Regen. cycles = Regeneration cycles
**Average ± standard deviation of three replicates.

Therefore, three cycles of flocculation and deflocculation were performed using the same nanocomposite to determine the reusability of the FCN for flocculants recycling. According to the data, the flocculation performance remained constant over the course of the three cycles of the flocculation/deflocculation process. This demonstrates that the properties of the FCN remain unchanged after multiple cycles of the treatment process.

As a result of these findings, it is anticipated that the ability of the synthesised nanocomposite to retain its flocculation capacity after several uses will aid in the reduction of operating costs associated with the use of these flocculants for water purification. It is clear that not only did the synthesised flocculant solve the water pollution problem, but it also recycled and reused contaminants numerous times, indicating that it has a great deal of potential in real-world applications.

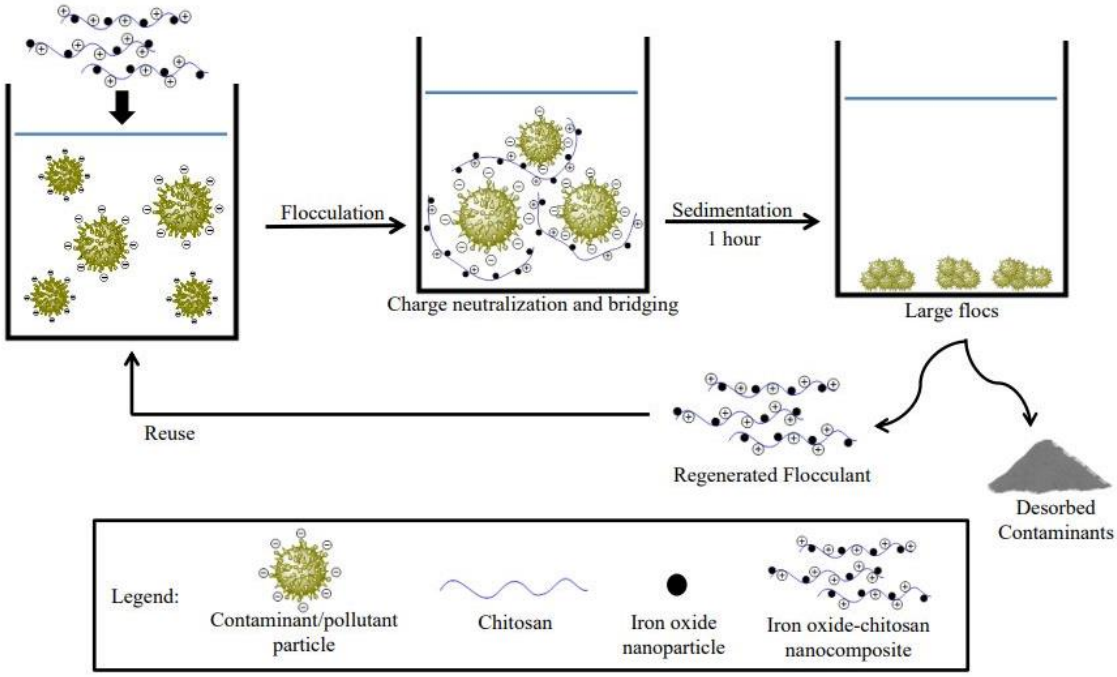


**Figure 8** Schematic representation of flocculation process in POME treatment using iron oxide-chitosan nanocomposite

### 3.4 Proposed Mechanism of Iron Oxide-Chitosan Nanocomposite

Technically, in the flocculation process, aspects such as particle surface charge and colloidal stability of wastewater colloids are important factors to consider when performing the flocculation process. In general, the cell walls of microorganisms and bacteria have a net negative charge when the pH of the environment is neutral [60].

The majority of water-suspended particles have a negative charge, and because they all have the same charge sign, they tend to repel one anotherwhen they come into contact [61]. Fats, waxes, sterols, and phospholipids are all types of lipids. Non-polar hydrocarbon structures are the building

blocks of lipids, and depending on the arrangement of long chain hydrocarbons and the presence or absence of a polar carboxylic acid in the structure, they can contain neutral, positively, or negatively charged components. For example, the study of olive mill wastewater conducted by Rytwo *et al*. [62] shown that the zeta potential value of the effluent are negatively charged. Figure 8 shows a schematic representation of flocculation process in POME treatment using oxide-chitosan nanacomposites.

## 4.0 CONCLUSION

FCN were successfully prepared and characterised, and they possess ideal characteristics as flocculants for POME pre-treatment. The spectrometry method results confirmed the binding of the ferrihydrite nanoparticle and chitosan, and also the contaminant uptake in POME after the flocculation. In comparison with chitosan and alum, the FCN showed excellent flocculation performance compared to others, with a removal efficiency of 72.38% turbidity, 77.32% TSS, 71.60% COD and 53.40% O&G at flocculant dosage of 1.5 g/L, pH 5 and 60 min settling time. Therefore, because the untreated POME had a pH of less than or around 5, the pH adjustment in the flocculation process of POME treatment with FCN can be neglected. Charge neutralisation and polymer bridging are the two major flocculation mechanisms for POME adsorption onto FCN. After flocculation, the FCN was regenerated and reused in three successive flocculation processes with new raw POME and showed magnificent performance with only a 1-2% drop in contaminant removal after three cycles and up to 80% flocculant recovery. The application of FC nanocomposite as a flocculant in water and wastewater treatment could significantly minimise the amount of contaminants while also providing eco-friendly flocculants for a safer environment.

## Conflicts of Interest

The author(s) declare(s) that there is no conflict of interest regarding the publication of this paper.

## Acknowledgement

The authors would like to thank FGV Oil Palm Industries Sdn. Bhd., Sungkai, Perak and the Department of Chemistry, Faculty of Science and Mathematics, Universiti Pendidikan Sultan Idris, Malaysia for providing research facilities to conduct this research.

## References

[1] Malaysian Palm Oil Council. 2022. Nutrition & Health. https://mpoc.org.my/nutrition-health.

[2] Kumaran, P., Hephzibah, D., Sivasankari, R., Saifuddin, N. and Sahamsuddin A. H. 2016. A Review on Industrial Scale Anaerobic Digestion Systems Deployment in Malaysia: Opportunities and Challenges. *Renewable and Sustainable Energy Reviews*. 56: 929-940. https://doi.org/10.1016/j.rser.2015.11.069.

[3] Adela, B. N., Muzzammil, N., Loh, S. K. and Choo, Y. M. 2014. Characteristic of Palm Oil Mill Effluent (POME) in an Anaerobic Biogas Digester. *Asian Journal of Mircobiology, Biotechnology & Environmental Sciences*. 16(1): 225-231.

[4] Jumadi, J., Kamari, A., Hargreaves, J. S. J. and Yusof. N. 2020. A Review of Nano-based Materials used as Flocculants for Water Treatment. *International Journal of Environmental Science and Technology*. 17: 3571-3594. https://doi.org/10.1007/s13762-020-02723-y.

[5] Bala, J. D., Lalung, J., Al-Gheethi, A. A. S., Kaizar, H. and Ismail, N. 2018. Reduction of Organic Load and Biodegradation of Palm Oil Mill Effluent by Aerobic Indigenous Mixed Microbial Consortium Isolated from Palm Oil Mill Effluent (POME). *Water Conservation Science and Engineering*. 3(3): 139-156. https://doi.org/10.1007/s41101-018-0043-9.

[6] Bashir, I., Lone, F. A., Bhat, R. A., Mir, S. A., Dar, Z. A. and Dar, S. A. 2020. Concerns and Threats of Contamination on Aquatic Ecosystems. *Bioremediation and Biotechnology: Sustainable Approaches to Pollution Degradation*. 1-26. https://doi.org/10.1007/978-3-030-35691-0_1.

[7] Kamyab, H., Chelliapan, S., Din, M. F. M., Rezania, S., Khademi, T. and Kumar, A. 2018. Palm Oil Mill Effluent as an Environmental Pollutant. In (Ed.). Palm Oil. IntechOpen. https://doi.org/10.5772/intechopen.75811.

[8] Chan, Y. J. and Chong M. F. 2019. Palm Oil Mill Effluent (POME) Treatment - Current Technologies, Biogas Capture and Challenges. In: Foo D., Tun Abdul Aziz M. (eds). Green Technologies for the Oil Palm Industry. Green Energy and Technology. Springer, Singapore. https://doi.org/10.1007/978-981-13-2236-5_4.

[9] Mohammad, S., Baidurah, S., Kobayashi, T., Ismail, N., and Leh, C. P. 2021. Palm Oil Mill Effluent Treatment Processes—A Review. Processes. 9(5): 739. https://doi.org/10.3390/pr9050739.

[10] Jumadi, J., Kamari, A., Abdul Rahim, N., Yusof, N., and Fatimah, I. 2022. Remediation of Palm Oil Mill Effluent (POME) using Selected Biological Techniques: A Mini Review. *Jurnal Teknologi*. 84(5): 93-103. https://doi.org/10.11113/jurnalteknologi.v84.18013.

[11] Yusoff, M. S., Aziz, H. A., Zamri, M. F. M. A., Suja', F., Abdullah, A. Z. and Basri, N. E. A. 2018. Floc Behavior and Removal Mechanisms of Cross-linked *Durio zibethinus* Seed Starch as a Natural Flocculant for Landfill Leachate Coagulation-Flocculation Treatment. *Waste Management*. 74: 362-372. https://doi.org/10.1016/j.wasman.2018.01.016.

[12] Halakarni, M., Mahto, A., Aruchamy, K., Mondal, D. and Nataraj, S. K. 2020. Developing Helical Carbon Functionalized Chitosan-based Loose Nanofiltration Membranes for Selective Separation and Wastewater Treatment. *Chemical Engineering Journal*. 417: 127911. https://doi.org/10.1016/j.cej.2020.127911.

[13] Brion-Roby, R., Gagnon, J., Deschênes, J. -S. and Chabot, B. 2018. Investigation of Fixed Bed Adsorption Column Operation Parameters using a Chitosan Material for Treatment of Arsenate Contaminated Water. *Journal of Environmental Chemical Engineering*. 6(1): 505-511. https://doi.org/10.1016/j.jece.2017.12.032.

[14] Halim, A. L. A., Kamari, A. and Phillip, E. 2018. Chitosan, Gelatin and Methylcellulose Films Incorporated with Tannic Acid for Food Packaging. *International Journal of Biological Macromolecules*. 120(Part A): 1119-1126. https://doi.org/10.1016/j.ijbiomac.2018.08.169.

[15] Yusoff, S. N. M., Kamari, A., Ishak, S. and Halim, A. L. A. 2018. *N*-hexanoyl-*O*-glycol Chitosan as a Carrier Agent for Water-insoluble Herbicide. *Journal of Physics: Conference Series*, 1097: 012053.

[16] França, D., Medina, Â. F., Messa, L. L., Souza, C. F. and Faez, R. 2018. Chitosan Spray-dried Microcapsule and Microsphere as Fertilizer Host for Swellable − Controlled Release Materials. *Carbohydrate Polymers*. 196: 47-55. https://doi.org/10.1016/j.carbpol.2018.05.014.
[17] Tripathi, N., Choppala, G., Singh, R. S. and Hills, C. D. 2017. Impact of Modified Chitosan on Pore Water Bioavailability of Zinc in Contaminated Soil. *Journal of Geochemical Exploration*. 186: 94-99. https://doi.org/10.1016/j.gexplo.2017.12.005.
[18] Yang, Z., Miao, H., Rui, Z. and Ji, H. 2019. Enhanced Formaldehyde Removal from Air using Fully Biodegradable Chitosan Grafted β-cyclodextrin Adsorbent with Weak Chemical Interaction. *Polymers*. 11(2): 276. https://doi.org/10.3390/polym11020276.
[19] Chik, C. E. N. C. E., Kurniawan, S. B., Shukri, Z. N. A., Terkula, I. B., Wahab, F., Endut, A., Lananan, F., Hasan, H. A., Abdullah, S. R. S., and Kasan, N. A. 2023. Chitosan Coagulant: Coagulation/Flocculation Studies on Turbidity Removal from Aquaculture Wastewater by Response Surface Methodology. *International Journal of Environmental Science and Technology*. https://doi.org/10.1007/s13762-023-04989-4.
[20] Saiyad, M., Shah, N., Joshipura, M., Dwivedi, A., and Pillai, S. 2023. Chitosan and its Derivatives in Wastewater Treatment Application. *Materials Today: Proceedings*. https://doi.org/10.1016/j.matpr.2023.10.157.
[21] Abdullah, N. H., Shameli, K., Abdullah, E. C. and Abdullah, L. C. 2018. Solid Matrices for fabrication of magnetic iron oxide nanocomposites: Synthesis, Properties, and Application for the Adsorption of Heavy Metal Ions and Dyes. *Composites Part B: Engineering*. 162: 538-568. https://doi.org/10.1016/j.compositesb.2018.12.075.
[22] Gutierrez, A. M., Dziubla, T. D. and Hilt, J. Z. 2017. Recent Advances on Iron Oxide Magnetic Nanoparticles as Sorbents of Organic Pollutants in Water and Wastewater Treatment. *Reviews on Environmental Health*. 32(1-2): 111-117. https://doi.org/10.1515/reveh-2016-0063.
[23] Chaiyarat, A. and Saejung, C. 2022. Photosynthetic Bacteria with Iron Oxide Nanoparticles as Catalyst for Cooking Oil Removal and Valuable Products Recovery with Heavy Metal Co-contamination. *Waste Management*. 140: 81-89. https://doi.org/10.1016/j.wasman.2022.01.005.
[24] Ali, A., Zafar, H., Zia, M., ul Haq, I., Phull, A. R., Ali, J. S. and Hussain, A. 2016. Synthesis, Characterization, Applications, and Challenges of Iron Oxide Nanoparticles. *Nanotechnology, Science and Applications*. 9: 49-67. https://dx.doi.org/10.2147%2FNSA.S99986.
[25] Wu, W., He, Q. and Jiang, C. 2008. Magnetic Iron Oxide Nanoparticles: Synthesis and Surface Functionalization Strategies. *Nanoscale Research Letters*. 3: 397. https://doi.org/10.1007/s11671-008-9174-9.
[26] Chisty, A. H., Rahman, M. M. 2022. Insight Of Iron Oxide-Chitosan Nanocomposites for Drug Delivery. In: Pandey, L.M., Hasan, A. (eds). Nanoscale Engineering of Biomaterials: Properties and Applications. Springer, Singapore. https://doi.org/10.1007/978-981-16-3667-7_22.
[27] Singh, S., Singh, G., and Bala, N. 2021. Synthesis and Characterization of Iron Oxide-hydroxyapatite-chitosan Composite Coating and Its Biological Assessment for Biomedical Applications. *Progress in Organic Coatings*. 150: 106011. https://doi.org/10.1016/j.porgcoat.2020.106011.
[28] Samejo, S., Baig, J. A., Uddin, S., Kazi, T. G., Afridi, H. I., Hol, A., Ali, F. I., Hussain, S., Akhtar, K., Perveen, S., and Bhutto, A. A. 2023. Green Synthesis of Iron Oxide Nanobiocomposite for the Adsorptive Removal of Heavy Metals from the Drinking Water. *Materials Chemistry and Physics*. 303: 127807. https://doi.org/10.1016/j.matchemphys.2023.127807.
[29] Sarojini, G., Kannan, P., Rajamohan, N., and Rajasimman, M. 2023. Bio-fabrication of Porous Magnetic Chitosan/$Fe_3O_4$ Nanocomposite using Azolla Pinnata for Removal of Chromium- Parametric Effects, Surface Characterization and Kinetics. *Environmental Research*. 218: 114822. https://doi.org/10.1016/j.envres.2022.114822.
[30] Jumadi, J., Kamari, A., Rahim, N. A., Wong, S. T. S., Yusoff, S. N. M., Ishak, S., Abdulrasool, M. M., and Kumaran, S. 2019. Removal of Methylene Blue and Congo Red by Magnetic Chitosan Nanocomposite: Characterization and Adsorption Studies. *Journal of Physics: Conference Series*. 1397: 012027. https://doi.org/10.1088/1742-6596/1397/1/012027.
[31] Villacís-García, M., Ugalde-Arzate, M., Vaca-Escobar, K., Villalobos, M., Zanella, R., and Martínez-Villegas, N. 2015. Laboratory Synthesis of Goethite and Ferrihydrite of Controlled Particle Sizes. *Boletín de la Sociedad Geológica Mexicana*. 67(3): 433-446.
[32] Pham, X. N., Nguyen, T. P., Pham, T. N., Tran, T. T. N., & Tran, T. V. T. 2016. Synthesis and Characterization of Chitosan-coated Magnetite Nanoparticles and Their Application in Curcumin Drug Delivery. *Advances in Natural Sciences: Nanoscience and Nanotechnology*. 7: 045010.
[33] Saritha, V., Srinivas, N. and Srikanth Vuppala, N. V. 2017. Analysis and Optimization of Coagulation and Flocculation Process. *Applied Water Science*. 7(1): 451-460. https://doi.org/10.1007/s13201-014-0262-y.
[34] Maćczak, P., Kaczmarek, H. and Ziegler-Borowska, M. 2020. Recent Achievements in Polymer Bio-based Flocculants for Water Treatment. *Materials*. 13(18): 3951. https://doi.org/10.3390/ma13183951.
[35] Hassan, M. A. A. and Puteh, M. H. 2007. Pre-treatment of Palm Oil Mill Effluent (POME): A Comparison Study using Chitosan and Alum. *Malaysian Journal of Civil Engineering*. 19(2): 128-141. https://doi.org/10.11113/mjce.v19.15747.
[36] Ahmed, I., Mondol, M. M. H., Lee, H. J. and Jhung, S. H. 2021. Application of Metal-organic Frameworks in Adsorptive Removal of Organic Contaminants from Water, Fuel and Air. *Chemistry - An Asian Journal*. 16(3): 185-196. https://doi.org/10.1002/asia.202001365.
[37] Nizamuddin, S., Siddiqui, M. T. H., Mubarak, N. M., Baloch, H. A., Abdullah, E. C., Mazari, S. A., Griffin, G. J., Srinivasan, M. P. and Tanksale, A. 2019. Iron Oxide Nanomaterials for the Removal of Heavy Metals and Dyes from Wastewater. *Nanoscale Materials in Water Purification*. 447-472. https://doi.org/10.1016/B978-0-12-813926-4.00023-9.
[38] Da Silva, S. B., Batista, G. L. and Santin, C. K. 2019. Chitosan for Sensors and Electrochemical Applications. *Chitin and Chitosan: Properties and Application*. 461-476. https://doi.org/10.1002/9781119450467.ch18.
[39] Guo, X., Qu, L., Zhu, S., Tian, M., Zhang, X., Sun, K. and Tang, X. 2015. Preparation of Three-dimensional Chitosan-graphene Oxide Aerogel for Residue Oil Removal. *Water Environment Research*. 88(8): 768-778. https://doi.org/10.2175/106143016x14609975747207.
[40] Ordaz-Díaz, L. A., Valle-Cervantes, S., Rodríguez-Rosales, J., Bailón-Salas, A. M., Madrid-Del Palacio, M., Torres-Fraga, K. and De la Peña-Arellano, L. A. 2017. Zeta Potential as a Tool to Evaluate the Optimum Performance of a Coagulation-flocculation Process for Wastewater Internal Treatment for Recirculation in the Pulp and Paper Process. *BioResources*, 12(3): 5953-5969. https://doi.org/10.15376/biores.12.3.5953-5969.
[41] Ganapathy, B., Yahya, A. and Ibrahim, N. 2019. Bioremediation of palm oil mill effluent (POME) using indigenous Meyerozyma guilliermondii. *Environmental Science and Pollution Research*. 26(11): 11113-11125. https://doi.org/10.1007/s11356-019-04334-8.
[42] Yu, W., Wang, C., Wang, G. and Feng, Q. 2020. Flocculation Performance and Kinetics of Magnetic Polyacrylamide Microsphere under Different Magnetic Field Strengths. *Journal of Chemistry*. 2020: 1579424. https://doi.org/10.1155/2020/1579424.
[43] Sivashankari, P. R. and Prabaharan, M. 2017. Deacetylation Modification Techniques of Chitin and Chitosan. *Chitosan Based Biomaterials*. 1: 117-133. https://doi.org/10.1016/B978-0-08-100230-8.00005-4.

[44] Nirmala, R., Il, B. W., Navamathavan, R., El-Newehy, M. H. and Kim, H. Y. 2011. Preparation and Characterizations of Anisotropic Chitosan Nanofibers via Electrospinning. *Macromolecular Research*. 19(4): 345-350. https://doi.org/10.1007/s13233-011-0402-2.

[45] Das, S. and Hendry, M. J. 2011. Application of Raman Spectroscopy to Identify Iron Minerals Commonly Found in Mine Wastes. *Chemical Geology*. 290(3-4): 101-108. https://doi.org/10.1016/j.chemgeo.2011.09.001.

[46] Rout, K., Mohapatra, M. and Anand, S. 2012. 2-line Ferrihydrite: Synthesis, Characterization and its Adsorption Behavior for Removal of Pd(II), Cd(II), Cu(II) and Zn(II) from Aqueous Solutions. *Dalton Transactions*. 41: 3302-12. https://doi.org/10.1039/C2DT11651K.

[47] Hanesch, M. 2009. Raman Spectroscopy of Iron Oxides and (oxy)hydroxides at Low Laser Power and Possible Applications in Environmental Magnetic Studies. *Geophysical Journal International*. 177(3): 941-948. https://doi.org/10.1111/j.1365-246X.2009.04122.x.

[48] Mazzetti, L. and Thistlethwaite, P. J. 2002. Raman Spectra and Thermal Transformations of Ferrihydrite and Schwertmannite. *Journal of Raman Spectroscopy*. 33(2): 104-111. https://doi.org/10.1002/jrs.830.

[49] Kunze, F., Kuns, S., Spree, M., Hülser, T., Schulz, C., Wiggers, H. and Schnurre, S. M. 2019. Synthesis of Silicon Nanoparticles in a Pilot-plant-scale Microwave Plasma Reactor: Impact of Flow Rates and Precursor Concentration on the Nanoparticle Size and Aggregation. *Powder Technology*. 342: 880-886. https://doi.org/10.1016/j.powtec.2018.10.042.

[50] Jakubowska, E., Gierszewska, M., Nowaczyk, J., and Olewnik-Kruszkowska, E. 2020. Physicochemical and Storage Properties of Chitosan-based Films Plasticized with Deep Eutectic Solvent. *Food Hydrocolloids*. 108: 106007. https://doi.org/10.1016/j.foodhyd.2020.106007.

[51] Grzybek, P., Jakubski, Ł., and Dudek, G. 2022. Neat Chitosan Porous Materials: A Review of Preparation, Structure Characterization and Application. *International Journal of Molecular Sciences*. 23(17): 9932. https://doi.org/10.3390/ijms23179932.

[52] Rabel, A. M., Jayanthi, V., Raj, N. N., Ramachandran, D. and Brijitta, J. 2013. Synthesis and Characterization of Chitosan-coated Iron Oxide Nanoparticles. *International Conference on Advanced Nanomaterials & Emerging Engineering Technologies*. 569-571. https://doi.org/10.1109/ICANMEET.2013.6609367.

[53] Asadpour, R., Sapari, N. B., Isa, M. H. and Orji, K. U. 2014. Enhancing the Hydrophobicity of Mangrove Bark by Esterification for Oil Adsorption. *Water Science and Technology*. 70(7): 1220-1228. https://doi.org/10.2166/wst.2014.355.

[54] Bala, J. D., Lalung, J. and Ismail, N. 2014. Biodegradation of Palm Oil Mill Effluent (POME) by Bacterial. *International Journal of Scientific and Research Publications*. 4(3): 1-10. http://repository.futminna.edu.ng:8080/jspui/handle/123456789/9852.

[55] Xing, Y., Li, X., Guo, X., Li, W., Chen, J., Liu, Q., Xu, Q., Wang, Q., Yang, H., & Bi, X. 2020. Effects of Different $TiO_2$ Nanoparticles Concentrations on the Physical and Antibacterial Activities of Chitosan-based Coating Film. *Nanomaterials*. 10(7): 1365. https://doi.org/10.3390/nano10071365.

[56] Bandi, S., Hastak, V., Pavithra, C. L. P., Kashyap, S., Singh, D. K., Luqman, S., Peshwe, D. R. and Srivastav, A. K. 2019. Graphene/chitosan-functionalized Iron Oxide Nanoparticles for Biomedical Applications. *Journal of Materials Research*. 34(20): 3389-3399. https://doi.org/10.1557/jmr.2019.267.

[57] El-kharrag, R., Abdel Halim, S. S., Amin, A. and Greish, Y. E. 2018. Synthesis and Characterization of Chitosan-coated Magnetite Nanoparticles using a Modified Wet Method for Drug Delivery Applications. *International Journal of Polymeric Materials and Polymeric Biomaterials*. 68(1-3): 73-82. https://doi.org/10.1080/00914037.2018.1525725.

[58] Magdziarz, A. and Werle, S. 2014. Analysis of the Combustion and Pyrolysis of Dried Sewage Sludge by TGA and MS. *Waste Management*. 34(1): 174-179. https://doi.org/10.1016/j.wasman.2013.10.033.

[59] Xiaohua, W. and Jiancheng, J. 2012. Effect of Heating Rate on the Municipal Sewage Sludge Pyrolysis Character. *Energy Procedia*. 14: 1648-1652. https://doi.org/10.1016/j.egypro.2011.12.1146.

[60] Igiri, B. E., Okoduwa, S. I. R., Idoko, G. O., Akabuogu, E. P., Adeyi, A. O. and Ejiogu, I. K. 2018. Toxicity and Bioremediation of Heavy Metals Contaminated Ecosystem from Tannery Wastewater: A Review. *Journal of Toxicology*. 2568038. https://doi.org/10.1155/2018/2568038.

[61] Prayogo, W., Siregar, J. P., Soewondo, P., Nasution, Z., Hanami, Z. A., Ikhwali, M. F., Estim, A. and Suryawan, I. W. K. 2023. The Investigation on Mineral Wool Performance as a Potential Filter to Remove TSS in Cikapayang River, East Jawa, Indonesia. *Environment and Natural Resources Journal*. 21(1): 9-18.

[62] Rytwo, G., Lavi, R., Rytwo, Y., Monchase, H., Dultz, S. and König, T. N. 2013. Clarification of Olive Mill and Winery Wastewater by Means of Clay–polymer Nanocomposites. *Science of The Total Environment*. 442: 134-142.